Marsh, D., Watts, A., & Knowles, P. F. (1976) *Biochemistry 15*, 3570-3578.
Martin, F. J., & MacDonald, R. C. (1976) *Biochemistry 15*, 321-327.
Mason, J. T., & Huang, C. (1978) *Ann. N.Y. Acad. Sci. 308*, 29-49.
Mayer, M. D., Hope, M. J., & Cullis, P. R. (1986) *Biochim. Biophys. Acta 858*, 161-168.
McLean, L. R., & Phillips, M. C. (1981) *Biochemistry 20*, 2893-2900.
McLean, L. R., & Phillips, M. C. (1984) *Biochemistry 23*, 4624-4630.
Nichols, J. W., & Pagano, R. E. (1981) *Biochemistry 20*, 2783-2789.
Nichols, J. W., & Pagano, R. E. (1982) *Biochemistry 21*, 1720-1726.
Parente, R. A., & Lentz, B. R. (1984) *Biochemistry 23*, 2353-2362.
Roseman, M. A., & Thompson, T. E. (1980) *Biochemistry 19*, 439-444.
Scotto, A. W., & Zakim, D. (1988) *J. Biol. Chem. 263*, 18500-18506.
Shaw, J. M., & Thompson, T. E. (1982) *Biochemistry 21*, 920-927.
Sheetz, M. P., & Chan, S. I. (1972) *Biochemistry 11*, 4573-4581.
Silvius, J. (1982) in *Lipid-Protein Interactions* (Jost, P., & Griffith, O. H., Eds.) Vol. 2, pp 239-281, Wiley, New York.
Taupin, C., Dvolaitzky, M., & Sauterey, C. (1975) *Biochemistry 14*, 4771-4775.
Thompson, T. E., & Huang, C. (1986) in *Physiology of Membrane Disorders* (Andreoli, T. E., Fanestic, D. D., Hoffman, J. J., & Schulz, S. G., Eds.) 2nd ed., pp 24-44, Plenum Press, New York.
Watts, A., Marsh, D., & Knowles, P. F. (1978) *Biochemistry 17*, 1792-1801.
Wimley, W. C., & Thompson, T. E. (1989) *Biophys. J. 55*, 114a.
Wong, M., & Thompson, T. E. (1982) *Biochemistry 21*, 4126-4132.

Gating Kinetics of pH-Activated Membrane Fusion of Vesicular Stomatitis Virus with Cells: Stopped-Flow Measurements by Dequenching of Octadecylrhodamine Fluorescence

Michael J. Clague, Christian Schoch, Loren Zech, and Robert Blumenthal*

Section on Membrane Structure and Function, LMMB, National Cancer Institute, National Institutes of Health, Building 10, Room 4B56, Bethesda, Maryland 20892

Received July 18, 1989; Revised Manuscript Received October 11, 1989

ABSTRACT: To identify the initial stages of membrane fusion induced by vesicular stomatitis virus, we performed stopped-flow kinetic measurements with fluorescently labeled virus attached to human erythrocyte ghosts that contained symmetric bilayer distributions of phospholipids. Fusion was monitored spectrofluorometrically using an assay based on mixing of the lipid fluorophore octadecylrhodamine. At 37 °C and pH values near the threshold for fusion, a lag phase of 2 s was observed. The lag time decreased steeply as the pH decreased, while the initial rate of fusion showed the reverse functional dependence on pH. The observed rapid fluorescence changes resulted from fusion of virus bound to the target, and the time lags were not due to association–dissociation reactions between virus and target. For a given pH value, the temperature dependence of the lag time was similar to that of the initial rate of fusion. The results were fitted to a multistate model similar to that resulting from ion channel gating kinetics. The model allows testing of hypotheses concerning the role of cooperativity and conformational changes in viral spike glycoprotein-mediated membrane fusion.

It is well established that spike glycoproteins on the viral membrane surface are responsible for the ability of enveloped viruses to invade host cells (White et al., 1983; Ohnishi, 1988). Vesicular stomatitis virus (VSV),[1] which normally first binds to the cell surface and then enters via the endocytic pathway, can be made to fuse to the plasma membrane by briefly lowering the pH of the medium after the virus has attached to the cell (White et al., 1981; Matlin et al., 1982; Blumenthal et al., 1987; Puri et al., 1988). A glycoprotein (G protein, M_r 60 000) is the sole membrane-spanning protein in VSV, of which about 1200 copies are expressed per virion (Thomas et al., 1985). A low pH (<6.6)-induced conformational change of this protein is thought to trigger the fusion event (Crimmins et al., 1983; Blumenthal, 1988).

To gain insight into the molecular mechanism of action of the viral spike glycoproteins, we examine the kinetics of lipid mixing as a result of fusion of membranes of virus and target. Over recent years, the octadecylrhodamine (R18) fluorescence dequenching assay has become a frequent means of monitoring membrane fusion (Hoekstra et al., 1984). One particularly useful aspect of this assay is its ability to facilitate the

[1] Abbreviations: VSV, vesicular stomatitis virus; R18, octadecylrhodamine B chloride; PBS, phosphate-buffered saline; MES, 4-morpholinoethanesulfonic acid; SAAM, simulation analysis and modeling.

quantitation of fusion between intact virions and target cell membranes (Stegmann et al., 1986; Blumenthal et al., 1987; Puri et al., 1988; Loyter et al., 1988). We use it here to study the kinetics of pH-dependent fusion of VSV prebound to "lipid-symmetric" erythrocyte ghosts. Normal erythrocytes are not very susceptible to fusion with VSV. However, it has recently been shown that a particular type of resealed erythrocyte ghost membrane can provide a suitable target for VSV (Grimaldi et al., 1988). We have chosen to use these ghosts, which have lost their asymmetric distribution of membrane lipid as a relatively simple model biological membrane, appropriate for this study. By using the stopped-flow technique, which ensures a rapid reduction in pH, we have obtained measurements of the initial stages of viral fusion as a function of pH and temperature. The compatibility of the data with a model for viral spike glycoprotein-induced membrane fusion (Blumenthal, 1988; Blumenthal et al., 1988; Puri et al., 1988) has been analyzed.

Experimental Procedures

Materials. Octadecylrhodamine B chloride (R18) was obtained from Molecular Probes (Eugene, OR). Fresh whole blood was obtained from the NIH Blood Bank and washed 3 times in phosphate-buffered saline (PBS), which consists of 137 mM NaCl, 2.7 mM KCl, 8.1 mM Na_2HPO_4, and 1.5 mM KH_2PO_4, at pH 7.4.

Preparation of Erythrocyte Ghosts with Symmetric Phospholipid Distribution. Resealed ghosts were prepared by hypotonic lysis at 4 °C, in 15 volumes of 10 mM Tris buffer, pH 7.4, containing 1 mM $MgCl_2$, 1 mM $CaCl_2$, 0.1 mM EGTA, and 0.1% BSA; after 2 min, isotonicity was restored by addition of concentrated buffer solution comprised of 150 mM Na_2HPO_4, 50 mM KH_2PO_4, 1.22 M NaCl, 30 mM KCl, 1 mM $CaCl_2$, and 1 mM $MgCl_2$. This suspension was then incubated at 37 °C for 40 min and subsequently washed 3 times in PBS. The procedure is based on that of Williamson et al. (1985), who reported that the resultant ghosts lose the asymmetric distribution of membrane lipids, characteristic to the human erythrocyte. We deviate from their procedure, primarily in using a higher lysis volume.

Labeling of Virus. Purified VSV (Indiana) was obtained from J. Brown (University of Virginia). The virus was grown on monolayer cultures of baby hamster kidney (BHK21) cells and purified by sucrose velocity and density gradients (Thomas et al., 1985). The pooled fraction of VSV contained approximately 0.4 mg of VSV protein/mL. Fourteen microliters of 1 mg/mL R18 in ethanol was added with rapid vortexing to 1 mL of purified virus. After incubation for 10 min at room temperature, free R18 was removed by elution of the labeled VSV from a Sephadex G25 PD-10 column (Pharmacia, Piscataway, NJ).

Binding to Cells. The labeled product of 1.5 mL of virus was incubated for 40 min at 4 °C with 5 mL of ghost suspension, containing 3×10^9 ghosts as determined by a Coulter Multisizer. The suspension was then washed twice in PBS and stored as a resuspended pellet of 5-mL volume. Prior to stop-flow experiments, the pellet was diluted 40-fold in PBS and stored on ice throughout the series. The virus:ghost ratio in the assay solution was approximately 100:1; this corresponds to a surface area ratio of about 1:37 and thus allows full R18 dequenching, while maximizing the initial observed signal.

Measurements of Rapid Kinetics. Stopped-flow dequenching assays were performed with an SFA-11 rapid kinetics accessory (Hi-Tech Scientific Ltd., Salisbury, England). The contents of two syringes were combined 1:1 to give the desired reaction mixture. One syringe contained the R18-VSV–ghost suspension in PBS, pH 7.4, while the other held PBS plus sufficient 4-morpholinoethanesulfonic acid (MES) to produce the required pH. The VSV–ghost suspensions were held at 37 °C and pH 7.4 for about 5 min before the reaction was triggered by mixing the thermostated suspensions into the observation cell within 50 ms. The reaction is monitored by using a Model 8000 spectrofluorometer (SLM Instruments Inc., Urbana, IL) in the fast kinetics mode at 560- and 590-nm excitation and emission, respectively. Ten data sets were averaged for each fast kinetics condition reported. In some experiments, fusion was monitored by the conventional R18 dequenching assay in the slow kinetics (1-s resolution) mode, which involves injection of a small volume of PBS/MES into a thermostated cuvette containing a stirred suspension of VSV–ghost complexes (Blumenthal et al., 1987; Puri et al., 1988; Grimaldi et al., 1988).

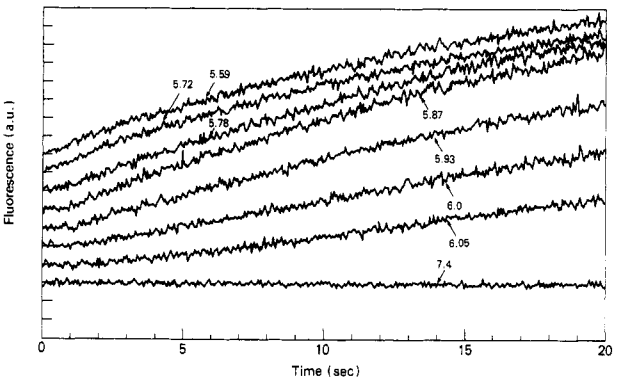

FIGURE 1: Rapid kinetics of fluorescence changes upon fusion of R18-labeled VSV with erythrocyte ghosts. The reaction was triggered by rapid mixing of equal volumes of an R18-VSV–ghost suspension and a PBS/MES solution at 37 °C as described in Experimental Procedures. Ten data sets were averaged for each pH indicated in the figure. Fluorescence at zero time, when the suspension was mixed, was the same for all pH values, but offset for clarity.

Results

Rapid Kinetics of VSV–Erythrocyte Ghost Fusion. Figure 1 shows the rapid kinetics of erythrocyte ghost–VSV fusion at eight pH values. Fluorescence changes were measured spectrofluorometrically with a 50-ms time resolution. At pH 6.05, no R18 dequenching was observed until 2 s after mixing. This lag time decreased steeply between pH 6.05 and 5.8, and at pH 5.6 it was not measurable with the time resolution employed. The rate of fluorescence change increased markedly in the same pH range. We interpret the lag time as reflecting the relative rates of rearrangements into the fusogenic state (see below). A single-exponential time course would show up as a linear curve on the semilogarithmic plot. However, we find that semilogarithmic plots of the data in Figure 1 are nonlinear (not shown). This multiexponential behavior will be taken into account when considering possible models for viral fusion (see Discussion).

Semilogarithmic plots were used to estimate initial slopes of the fluorescence changes in Figure 1. The pH dependence of the rates (Figure 2A) and delays (Figure 2B) was very similar to the pH dependence of fusion measured previously (White et al., 1981; Florkiewitz & Rose, 1984; Yamada & Ohnishi, 1986; Blumenthal et al., 1987) with the steepest change between pH 6.05 and 5.8.

To examine the levels of fusion reached after longer times, we mixed equal volumes of the R18-VSV–ghost suspension and PBS/MES at 37 °C and various pH values and measured fluorescence dequenching after 2.5 h of incubation. Figure 2C shows extents for single time points (2.5 h) as a function

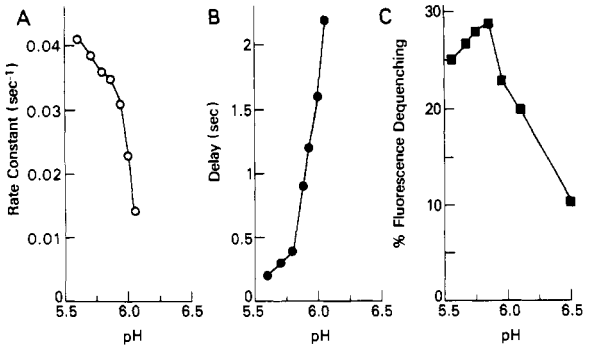

FIGURE 2: pH dependence of fusion of VSV with erythrocyte ghosts. (A) The rates of fluorescence change as a function of pH were calculated from maximal slopes of kinetic curves shown in Figure 1. (B) The delays as a function of pH were calculated from the time lags for the onset of fluorescence change of the kinetic curves shown in Figure 1. (C) Equal volumes of the R18-VSV–ghost suspension and PBS/MES were mixed at 37 °C and various pH values, and fluorescence dequenching was measured after 2.5 h of incubation.

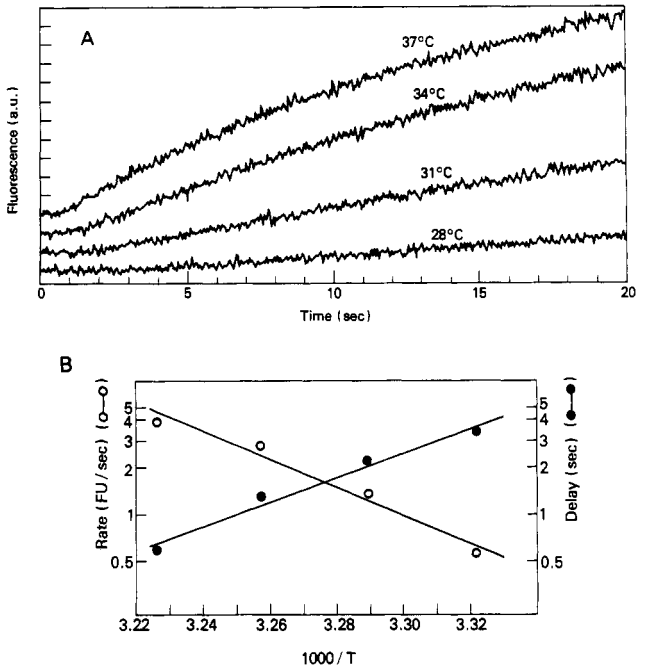

FIGURE 3: Temperature dependence of fusion of R18-labeled VSV with erythrocyte ghosts. (A) The reaction was triggered by rapid mixing of equal volumes of an R18-VSV–ghost suspension and a PBS/MES solution at pH 5.85 and different temperatures. Ten data sets were averaged for each temperature indicated in the figure. Fluorescence at zero time, when the suspension was mixed, was the same for all temperatures but offset for clarity. (B) Arrhenius plots for delays and rates calculated from the data presented in (A).

of pH. A similar pH dependence of "extent" was apparent at shorter times (15 min) of incubation (data not shown). The pH dependence of the extent of fusion of VSV does not appear to be as steep as that of the rate and lag (cf. Figure 2A and Figure 2B). Moreover, the curve appeared to be bell-shaped with a maximum at about pH 5.8. Such bell-shaped curves have also been observed for the extent fusion of VSV with HERL 66 cells after 10 min at 37 °C (Yamada & Ohnishi, 1986). The observation that the level of fusion is not the same for all pH values even after incubation at longer times (Figure 2C) will be taken into account in a proposed model which accounts for the kinetic data (see below).

Temperature Dependence. Figure 3A shows the temperature dependence of VSV–ghost fusion at pH 5.83 monitored by rapid kinetics. The effect of reducing the temperature (Figure 3) is to increase the length of the lag phase, and reduce

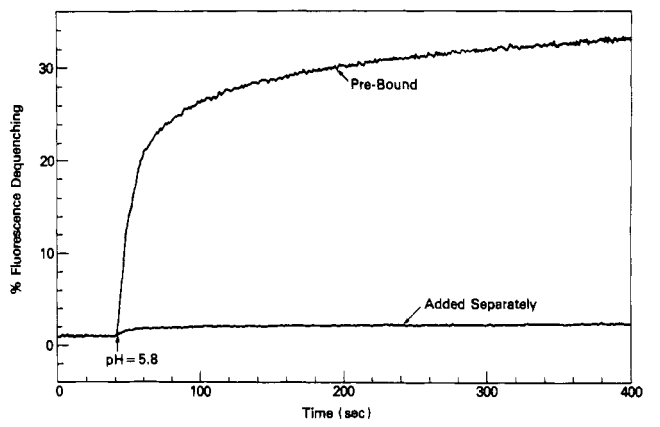

FIGURE 4: Effect of association on VSV–erythrocyte ghost fusion kinetics. Prebound R18-VSV–ghost complexes or R18-VSV and ghosts separately added were incubated in 2 mL of PBS, pH 7.4, at 37 °C. At about 40 s, the pH in the medium was changed to 5.83 by adding 25 μL of 1 M MES indicated by the arrow.

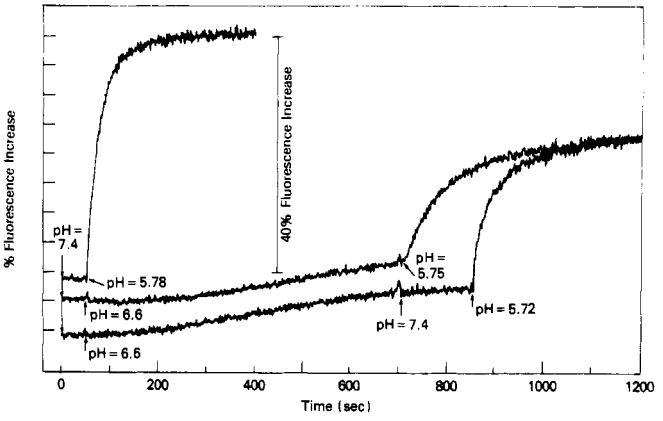

FIGURE 5: Inactivation during fusion. R18-VSV–ghost complexes were incubated in 2 mL of PBS, pH 7.4, at 37 °C. In the top curve, the pH in the medium was changed to 5.78 at about 50 s; in the middle curve, the pH in the medium was changed to 6.6 at 50 s, and to pH 5.75 after 700 s; in the bottom curve, the pH in the medium was changed to 6.6 at 50 s, back to pH 7.4 after 700 s, and finally to 5.72 after 850 s.

the rate of fusion. The delays and rates are presented in Figure 3B as an Arrhenius plot. Both the rates and delays of fluorescence dequenching were linear over the range studied with activation energies of 42 and 36 kcal/mol, respectively. The similar temperature dependence of rates and delays indicates that both parameters incorporate features of the same process.

Virus–Cell Association and Fusion. We assume that the fusion event we observe is dominated by virus bound to the membrane at the time of mixing and that we can thus neglect consideration of diffusion-limited virus–cell association in our analysis. To examine this issue, we compared fusion triggered when virus was prebound to ghosts with fusion when virus and ghosts were added together without prebinding. In the latter case, virus and ghosts have to associate by random collisions before undergoing the process of fusion itself. In these experiments, fusion was monitored by the conventional R18 dequenching assay in the slow kinetics (1 s) mode, after lowering the pH by injection of a small volume of PBS/MES into a thermostated cuvette containing a stirred suspension of VSV and ghosts (Blumenthal et al., 1987; Puri et al., 1988; Grimaldi et al., 1988). When virus is prebound to ghosts, we observed 30–40% fluorescence dequenching after 400 s (Figure 4). On the other hand, when virus and ghosts were separately added, the final level of fluorescence dequenching was less than 5%

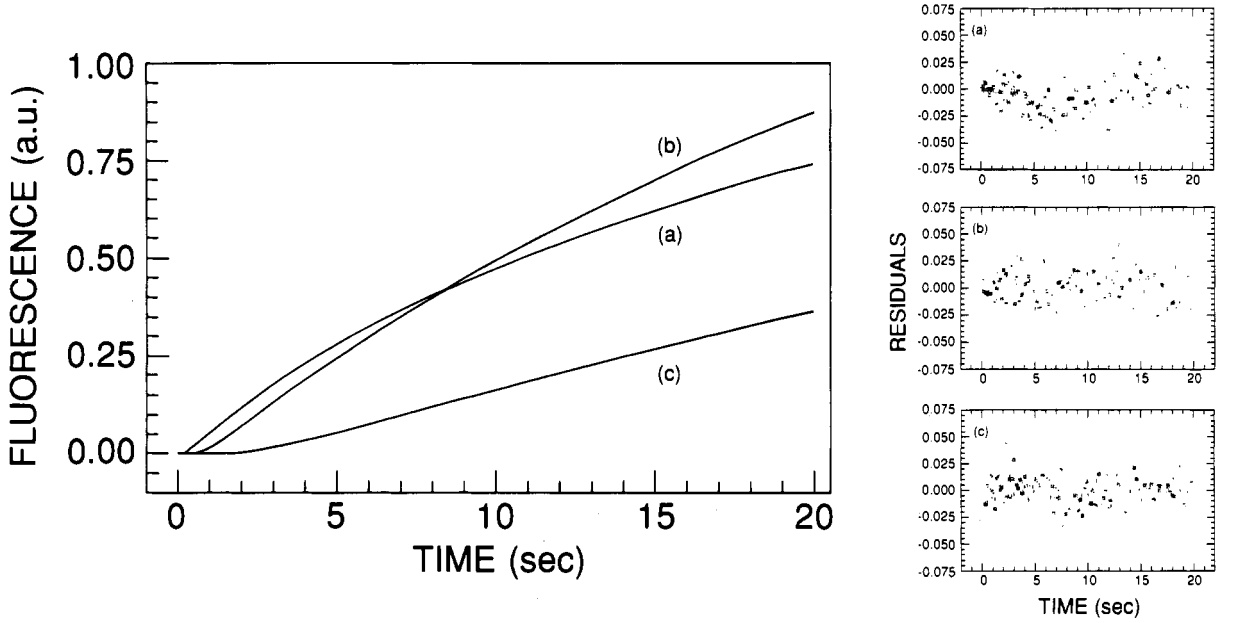

FIGURE 6: Curves fitted to kinetic data. The data at (a) pH 5.59, (b) pH 5.87, and (c) pH 6.05 were simultaneously fitted to Scheme II using SAAM (Berman et al., 1983). The restraint that $T \leftrightarrow R_0$ transitions are pH independent was imposed. Values attained for the various rate constants are listed in Table I. The three curves are drawn by using those rate constants. Residuals are shown on the right panels.

of the prebound value. As the latter followed the same kinetics as prebound virus, we assume that the 5% is due to virus bound in the time before pH reduction (2.5 min). This experiment indicates that the rapid kinetics observed in Figures 1 and 3 are dominated by fusion of VSV prebound to ghost membranes.

"Inactivation" during Fusion. One possible explanation of the variation of extent of fusion with pH (see Figure 2C) could be that "inactivation" occurs during the fusion reaction. To examine this possibility, we monitored the extent of fusion attained at pH 5.8 before and after exposing the VSV–ghost complexes to pH 6.6 (Figure 5). When the VSV–ghost complexes were kept at 7.4 for 50 s, there was 41% fluorescence dequenching upon lowering the pH to 5.78. On the other hand, incubation of the complexes for 650 s at pH 6.6 resulted in only 22% fluorescence dequenching. Moreover, the initial rate was lowered after the pH 6.6 exposure. Partial restoration of activity could be achieved by returning to pH 7.4 for 150 s after exposure at pH 6.6 for 650 s. This indicates that the "inactivation" process has a reversible component. An interpretation of these data in terms of a channel gating model with densensitization will be presented below.

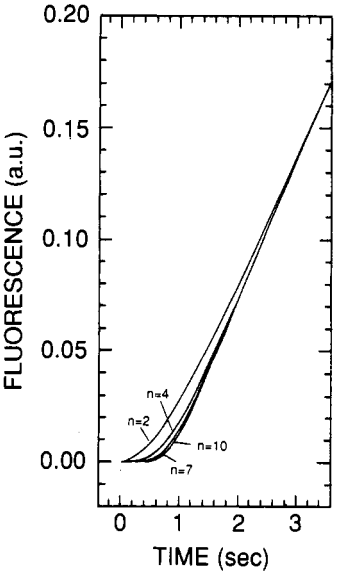

FIGURE 7: Curves fitted to the delay. The rate constants for the curve fitted at pH 5.87 are from Table I. Curves are shown with different numbers (n) of R states: from left to right, n = 2, 4, 7, and 10.

DISCUSSION

Measurement of Viral Membrane Fusion by Stopped-Flow Kinetics. In this paper, we demonstrate for the first time that the kinetics of viral fusion can be measured directly and continuously using stopped-flow mixing techniques. Previously, the R18 assay had been used to measured kinetics of VSV–cell fusion (Blumenthal et al., 1987; Puri et al., 1988). However, the conventional method of performing the assay, by the injection of a pH-lowering solution into a stirred cuvette, does not allow resolution of induced fluorescence changes within the first 3–4 s. By obtaining particularly well-resolved data for early time points, we are able to gain further information about the initial events in viral spike glycoprotein-mediated fusion. In defining membrane fusion, it is necessary to establish the continuity of the aqueous compartments defined by the membranes and the lipid compartments comprising the membranes of two previously separated structures (Blumenthal, 1987), and, therefore, we do not prejudge the fusion mechanism to be one of "lipid channeling". However, at the present time, the redistribution of the lipid probe is the only measurement that can be made with intact virus. Core mixing could potentially be measured by using reconstituted viral envelopes (Paternostre et al., 1989), but that measurement might be compromized by leakage during fusion.

We wish to emphasize the importance of measuring fusion of virus prebound to the target membrane. If the virus and target are added separately, the complexity of the "gating" process is masked by having to consider association and dissociation reactions, and little information about the initial events of fusion will be gained. In their study of fusion of influenza virus (X-47 strain) with erythrocyte ghosts, Stegmann et al. (1986) observed a lag phase if the virus was added to the ghosts without prebinding. That lag disappeared if virus and ghost were prebound, indicating that the lag was due to association–dissociation reactions. In the experiment in Figure

4, fusion was very ineffective if VSV and ghosts were not allowed to prebind before the pH was lowered. This might be due to the fact that the virus–ghost collisions leading to fusion are very inefficient with VSV.

On the basis of simple diffusion considerations, the $t_{1/2}$ for dispersal of the lipid probe from the virus after establishment of membrane continuity is <20 ms. It is therefore unlikely that probe diffusion is rate-limiting at 37 °C or at lower temperatures. Moreover, since delays occur before the onset of membrane fusion, they are not affected by probe diffusion. Since the diffusion coefficient of lipids changes by a factor of about 2 between 25 and 37 °C (Edidin, 1987), it is unlikely that diffusion plays a role in the temperature dependence of the rate constants (Figure 3).

Analysis of the Rapid Kinetic Data. A gating model for viral spike glycoprotein-mediated membrane fusion (Blumenthal, 1988; Blumenthal et al., 1988, 1989; Puri et al., 1988) has previously been formulated as Scheme I.

Scheme I

$$T_0 \leftrightarrow R_0 \rightarrow R_1 \ldots \rightarrow R_n$$

In the model represented in Scheme I, oligomeric clusters of viral spike glycoproteins are assumed to undergo a conformational change from a T_0 state to an R_0 state. Protonation shifts the oligomer from R_0 via R_1, R_2, ... etc. to R_n, the "fusogenic" state. The observed rates of R18 dequenching from the stopped-flow data of Figure 1 can be fitted to the model of Scheme I by varying the rate constants for the conformational transitions. We fitted these data at various pH values using the Simulation Analysis and Modeling (SAAM) package developed by Berman et al. (1983). From our first attempts at fitting the data, it became obvious that Scheme I provides an inadequate description. An improved model incorporating the following features can satisfy all the data collected: (1) To satisfy the time lag, the viral proteins must go through multiple states, R_1, R_2, ..., etc., prior to the final fusogenic state (R_n). (2) After the initial lag, the fluorescence increase cannot be described by a single exponential (see Figure 1). To account for this multiexponential behavior, we hypothesize that a $T_0 \leftrightarrow R_0$ equilibrium is established prior to pH-triggering. Our data are compatible with about 20% initially in the R_0 state. (3) A scheme with pH-dependent rate constants for the R_1, R_2, ..., R_n transitions would lead to the same extent of fusion irrespective of pH, since all would eventually end up in the R_n state which is fusogenic. However, to account for the fact that the extents of fusion are pH-dependent, we invoke an "inactivation" pathway which involves protonations of the T state to form the D (desensitized) state.

The present model incorporating the above constraints is shown in Scheme II. We simultaneously fitted the observed rates of R18 dequenching from the stopped-flow data of Figure 1 at pHs 6.05, 5.87, and 5.59 to the model of Scheme II by varying the rate constants for the conformational transitions shown in the scheme. Although for such a multiparameter system there is no unique solution, we can achieve a satisfactory fit incorporating the following features (see Figures 6 and 7): (i) $T_0 \leftrightarrow R_0$ transitions are pH-independent; (ii) $R_0 \rightarrow \ldots \rightarrow R_n$ and $T \rightarrow D$ rates increase with decreasing pH; and (iii) the delay is consistent with six transitions until the final open state, R_7, is reached.

Figure 6 shows the calculated curves for the three pH values. The parameters used for the fits are summarized in Table I.

Scheme II

$$D_m \leftarrow \ldots D_1 \leftrightarrow T_0 \leftrightarrow R_0 \rightarrow R_1 \ldots \rightarrow R_n$$

Figure 7 shows the effect of adding states to the $R_0 \rightarrow \ldots \rightarrow R_n$ pathways, which determine the delay characteristics. As more compartments are added and delay rates are suitably adjusted, a sharper rise in fluorescence can be accommodated. To obtain a good fit to the whole curve with $n = 2$ or 4 yields a poor fit to the delay. Optimal fits to the delay were achieved with $n = 7$ with no significant improvement when more compartments are added. Figure 7 illustrates this point for the pH 5.87 data. As the progression to D_m is relatively slow, a one-compartment reversible inactivation pathway is sufficient to describe the curves within our chosen time frame, and the values shown in Table I for the $T \leftrightarrow D$ transitions are poorly determined. We could substitute $R_0 \leftrightarrow D$ transitions for the $T \leftrightarrow D$ transitions with similar fits to experimental curves.

Interpretation of the Model. The multiple-state gating feature accounts for the observed time lag. In drawing the analogy with ion channel gating kinetics, the T and R_1–R_6 states in Scheme II represent closed states and the D states desensitized states, whereas the R_7 state represents the fully liganded open state of the channel. In studies of ion channel kinetics, no time lags have been observed even in the millisecond range (Hess et al., 1987; Karpen et al., 1988). Mechanisms involving protein association following ligand binding are too slow to account for the observed kinetics in that case. This is consistent with the notion that the subunits constituting the ion channel are already prearranged to form the ion channel (Changeux et al., 1984). However, processes involving the time lag in this study might very well be due to protein aggregation. This is consistent with pH-dependent oligomerization of VSV G protein determined by sucrose-gradient centrifugation (Doms et al., 1987), and with the electron microscopic observation that the G proteins migrate to the poles of VSV in response to a reduction of pH (Brown et al., 1988). The lag is likely to be a function of the lateral diffusion coefficient of the G protein, its surface density, and the probability of a collision between two complexes leading to a stable oligomer. Only the latter would we expect to be pH dependent. In the best curve fits of the data to the model, the fusogenic state is associated with six protonations. Although Hill plots (Blumenthal, 1988) and radiation inactivation analysis (Bundo-Morita et al., 1988) suggested that the functional unit for fusion is comprized of a number of G-protein molecules, this is the first experimental demonstration that the fusion process undergoes a series of activation steps.

The general patterns expressing extents of fusion as a function of pH shown in Figure 2C are well explained by this model. In the case of influenza virus, the extents of fusion also appeared to be pH dependent (Yoshimura et al., 1982). Those overall extents are derived from a balance between two competing pathways: the transitions leading to the fusogenic state (R_n) and the transition leading to the inactive state (D_1). We have depicted the latter pathway as reversible. However, the "inactivation" pathway is also likely to be a multistep process with some irreversible steps. The different pH dependence of the rates through those two pathways leads to an optimal "extent" at pH 5.8 shown in Figure 2C. In the case of ligand-activated ion channels, similar time- and ligand-dependent transitions to inactive forms have been observed (Changeux et al., 1984; Hess et al., 1987).

The $T_0 \leftrightarrow R_0$ distributions as an initial condition to describe the kinetics is consistent with the notion that the unprotonated R form is not fusion-competent. This is supported by the

Table I: Rate Constants Obtained from SAAM Analysis, for Which Resultant Curves Are Shown in Figure 6[a]

transition	rate constants (s^{-1})		
	pH 6.05	pH 5.87	pH 5.59
$R_0 \rightarrow R_1$	0.0525	0.195	0.35
$R_1 \rightarrow R_2 \ldots \rightarrow R_7$	2.75	6.55	32.1
$T_0 \rightarrow R_0$	0.057	0.057	0.057
$R_0 \rightarrow T_0$	0.147	0.147	0.147
$T_0 \rightarrow D_1$	0.01	0.011	0.074
$D_1 \rightarrow T_0$	0.4	0.3	0.1

[a] Values for T ↔ D transitions are poorly defined at pH 5.87 and 6.05 (see text).

observation (Puri et al., 1988) that incubation of VSV at low pH prior to binding to cells leads to significant enhancement of membrane fusion at low pH (R_n state) but not to fusion at neutral pH (R_0 state). The inactivation of VSV bound to target might appear contradictory to the phenomenon of pH activation of unbound virus. However, VSV bound to target cells and subsequently exposed at 4 °C to the low pH did not show pH activation of fusion (Puri et al., 1988). One possibility is that different initial states represent different degrees of apposition with the target membrane, of which only the most advanced can enter into a fusogenic state. This implies that the G protein is required to undergo its conformational change while bearing a distinct spatial relationship with the target membrane. In that sense, one can regard the R state as the appropriately apposed virus, whereas the T state represents inappropriate apposition. Inactivation might then be a result of the viral proteins undergoing conformational changes while the virus is in a position inappropriate for fusion. Therefore, we observe little fusion without prebinding (see Figure 4). This would satisfy an elegant feature of the model, namely, that inactivation proceeds from a different state than fusion; thus, the same conformational changes could underpin both events.

In conclusion, we have here demonstrated the applicability of the stopped-flow technique for measuring viral fusion with a biological membrane. In doing so, we have been able to show a level of complexity of the event, impossible using slower data acquisition methods. Using the framework of our kinetic data, we have suggested novel hypotheses for factors relevant to the fusion process, consistent with a model of minimal complexity giving an adequate description of the data.

ACKNOWLEDGMENTS

We thank Dr. Andreas Herrmann for many helpful suggestions.

Registry No. R18, 65603-19-2; H^+, 12408-02-5.

REFERENCES

Berman, M., Beltz, W. F., Greif, P. C., Chabay, R., & Boston, R. C. (1983) *Consam User's Guide*, National Institutes of Health, Bethesda, MD.

Blumenthal, R. (1987) *Curr. Top. Membr. Transp. 29*, 203–254.

Blumenthal, R. (1988) *Cell Biophys. 12*, 1–12.

Blumenthal, R., Bali-Puri, A., Walter, A., Covell, D., & Eidelman, O. (1987) *J. Biol. Chem. 262*, 13614–13619.

Blumenthal, R., Puri, A., Walter, A., & Eidelman, O. (1988) in *Molecular Mechanisms of Membrane Fusion* (Ohki, S., Doyle, D., Flanagan, T., Hui, S. W., & Mayhew, E., Eds.) pp 367–383, Plenum Press, New York.

Blumenthal, R., Puri, A., Sarkar, D. P., Chen, Y., Eidelman, O., & Morris, S. J. (1989) *UCLA Symp. Mol. Cell. Biol., New Ser. 90*, 197–217.

Brown, J. C., Newcomb, W. W., & Lawrenz-Smith, S. (1988) *Virology 167*, 625–629.

Bundo-Morita, K., Gibson, S., & Lenard, J. (1988) *Virology 163*, 622–624.

Changeux, J.-P., Devillers-Thiery, A., & Chemoulli, P. (1984) *Science 225*, 1335–1345.

Crimmins, D. L., Mehard, W. B., & Schlesinger, S. (1983) *Biochemistry 22*, 5790–5796.

Doms, R. W., Keller, D. S., Helenius, A., & Balch, W. E. (1987) *J. Cell Biol. 105*, 1957–1969.

Edidin, M. (1987) *Curr. Top. Membr. Transp. 29*, 91–127.

Florkiewicz, R. Z., & Rose, J. K. (1984) *Science 225*, 721.

Grimaldi, S., Verna, R., Puri, A., Morris, S. J., & Blumenthal, R. (1988) *Serono Symp. Publ. 51*, 197–211.

Hess, G. P., Udgaonkar, J. B., & Olbricht, W. L. (1987) *Annu. Rev. Biophys. Biophys. Chem. 16*, 507–534.

Hoekstra, D., de Boer, T., Klappe, K., & Wilschut, J. (1984) *Biochemistry 23*, 5675–5681.

Karpen, J. W., Zimmerman, A. L., Stryer, L., & Baylor, D. A. (1988) *Proc. Natl. Acad. Sci. U.S.A. 85*, 1287–1291.

Loyter, A., Citovsky, V., & Blumenthal, R. (1988) *Methods Biochem. Anal. 33*, 128–164.

Matlin, K. S., Reggio, H., Helenius, A., & Simons, K. (1982) *J. Mol. Biol. 156*, 609–631.

Ohnishi, S. (1988) *Curr. Top. Membr. Transp. 32*, 257–296.

Paternostre, M., Lowy, R. J., & Blumenthal, R. (1989) *FEBS Lett. 243*, 251–258.

Puri, A., Winick, J., Lowy, R. J., Covell, D., Eidelman, O., Walter, A., & Blumenthal, R. (1988) *J. Biol. Chem. 263*, 4749–4753.

Stegmann, T., Hoekstra, D., Scherphof, G., & Wilschut, J. (1986) *J. Biol. Chem. 261*, 10966–10969.

Thomas, D., Newcomb, W. W., Brown, J. C., Wall, J. S., Hainfeld, J. F., Trus, B. L., & Steven, A. C. (1985) *J. Virol. 54*, 598–607.

White, J., Matlin, K., & Helenius, A. (1981) *J. Cell Biol. 89*, 674–679.

White, J., Kielian, M., & Helenius, A. (1983) *Q. Rev. Biophys. 16*, 151–195.

Williamson, P., Algarin, L., Bateman, J., Choe, H. R., & Schlegel, R. A. (1985) *J. Cell. Physiol. 123*, 209–214.

Yamada, S., & Ohnishi, S. (1986) *Biochemistry 25*, 3703–3708.

Yoshimura, A., Kuroda, K., Kawasaki, K., Yamashina, S., Maeda, T., & Ohnishi, S. (1982) *J. Virol. 43*, 284–293.